Geochimica et Cosmochimica Acta 336 (2022) 177–187

Contents lists available at ScienceDirect

Geochimica et Cosmochimica Acta

journal homepage: www.elsevier.com/locate/gca

Supernova versus cosmic ray origin for exotic nuclides in geomaterials: A test using ^{3}He with ^{60}Fe in marine sediments

David W. Graham *, Kevin Konrad [1]

College of Earth, Ocean, and Atmospheric Sciences, Oregon State University, Corvallis, OR 97331 USA

ARTICLE INFO

Article history:
Received 16 March 2022
Accepted 12 September 2022
Available online 17 September 2022
Associate editor: Franco Marcantonio

Keywords:
Supernova
Galactic cosmic rays
Helium isotopes
^{3}He
^{60}Fe
Interplanetary dust

ABSTRACT

We report ^{3}He and ^{4}He concentrations in 57 sediment samples from the southeast Indian Ocean where ^{60}Fe excesses were previously identified in a subset of the same samples (Wallner et al., 2016). The coupled ^{60}Fe-^{3}He data allow further evaluation of two competing hypotheses: (1) a nearby supernova (SN) showered Earth with exotic radionuclides such as ^{60}Fe during the last 3 million years, or (2) ^{60}Fe in terrestrial archives was generated by reactions of galactic cosmic rays (GCRs) on micrometeorite grains that were irradiated for hundreds of millions of years in the interstellar medium, where ^{3}He production by GCRs is larger than the solar wind ^{3}He flux.

Piston core ELT49-53 sediments show no correlation between ^{3}He and ^{60}Fe, and sedimentary ^{3}He appears to be dominated by the presence of interplanetary dust particles (IDPs). Because ^{3}He is not supplied in significant amounts by SN ejecta, the absence of a ^{3}He-^{60}Fe correlation provides additional, although circumstantial evidence for the supernova hypothesis. Large uncertainties in the relatively small number of sediment ^{60}Fe measurements currently limit a firmer conclusion.

The extraterrestrial ^{3}He accumulation rate in ELT49-53 from 3.2 to 1.7 Ma was $0.88 \pm 0.26 \times 10^{-12}$ cm^3 STP/g/kyr, similar to IDP ^{3}He flux estimates from previous sedimentary and ice core records that span both shorter and longer time scales. ^{4}He and ^{60}Fe accumulation rates during this time interval were $0.11 \pm 0.04 \times 10^{-6}$ cm^3 STP/cm^2/kyr and $1.9 \pm 0.5 \times 10^4$ atoms/cm^2/kyr. Bulk sediment [^{4}He] is strongly anti-correlated with sediment $CaCO_3$ content, evidence for modulation of the terrigenous and cosmic sedimentary fractions primarily by changes in biogenic carbonate deposition. Although the dominant terrigenous source has not been uniquely identified at the Indian Ocean deposition site, it resembles eolian material from the continental interior of Australia, and shows a narrow range of ^{3}He/^{4}He (from 2 to 4×10^{-8}, 0.015–0.030 R_A) over the last ~3 Myrs.

1. Introduction

The discovery of live ^{60}Fe in terrestrial samples led to the idea that a nearby supernova (SN) showered the Earth with exotic nuclides in the last few million years (Ellis et al., 1996; Fields and Ellis, 1999; Fields et al., 2005; Knie et al., 1999, 2004; Fields et al., 2019). The timing of the most recent SN event is proposed to be between 1.7 and 3.2 Ma, leading to the notion that it could have been responsible for the transition from Pliocene to Pleistocene climatic conditions on Earth (Ludwig et al., 2016; Thomas et al., 2016). However, in the one case where a further test of this hypothesis was carried out using ^{3}He measurements in the same ferromanganese crust studied for ^{60}Fe, Basu et al. (2007) and Stuart and Lee (2012) argued strongly against the supernova hypothesis (see Section 2). Their alternative hypothesis is that the ^{60}Fe-excess was derived from galactic cosmic ray (GCR) production in micrometeorites during an extended passage of hundreds of millions to billions of years through the interstellar medium. More recent studies of ^{60}Fe, in marine sediments that offer a far better temporal resolution than ferromanganese crusts, clearly show a strong peak in ^{60}Fe between 3.2 and 1.7 Ma (Ludwig et al., 2016; Wallner et al., 2016). Wallner et al. (2016) claim that this signal resulted from a nearby supernova, and that the results exclude the possibility of a micrometeorite source of ^{60}Fe because the cosmic dust flux is 400 times less than required from the new sediment data. The objective of the present study is to further evaluate the ^{60}Fe record in marine sediments of this age by analyzing the same samples for ^{3}He.

* Corresponding author.
E-mail address: david.graham@oregonstate.edu (D.W. Graham).
[1] Present address: Department of Geoscience, University of Nevada, Las Vegas, Las Vegas, NV 89154.

https://doi.org/10.1016/j.gca.2022.09.016
0016-7037/

2. Background

2.1. ^{60}Fe and the Supernova Hypothesis

The early search for terrestrial archives of SN ejecta stemmed from both astrophysical observations and theoretical calculations. Observations had been made of a young nearby SN remnant. Theoretical estimates also showed that a SN explosive event occurs within ~100 pc of the solar system every few million years (1 parsec = 1 parallax second and corresponds to the distance at which 1 astronomical unit - the mean radius of Earth's orbit around the sun - or AU, subtends an angle of 1 s of arc. One pc is equivalent to 3.26 light years or 3.09×10^{13} km, and is a typical spacing of neighboring stars in our galaxy, which has a size of ~10^4 pc). Thus the prediction was made that geochemical anomalies associated with the SN events might be found on Earth (e.g., Ellis et al., 1996; Fields and Ellis, 1999). ^{60}Fe was the most promising isotope for the terrestrial search because it is produced in significant amounts by supernovae. It also has a sufficiently long half-life to survive the transport to Earth, modeled to be ~100–400 kyr for a SN event at 100 pc (Fry et al., 2015). This ^{60}Fe was assumed to be derived from SN events within the so-called Local Bubble. This is a diffuse region of hot X-ray emitting plasma surrounded by a shell of cold gas and dust, and has a radius of ~200 pc. The solar system entered the Local Bubble ~5 million years ago and is now embedded within it. The Local Bubble is thought to originate from ~20 SN explosions that occurred during the last 14 Myrs, within a moving group of stars whose remnants are now found mostly lying on the Local Bubble surface (Benitez et al., 2002; Zucker et al., 2020).

For stellar masses between 8 and 25 times that of the sun ($M_\odot$), SN events eject about 0.5-14 $\times$ 10^{-5} $M_\odot$ of ^{60}Fe, depending on the progenitor mass (Woosley and Weaver, 1995; Rauscher et al., 2002; Limongi and Chieffi, 2006). Wallner et al. (2016) deduced that the terrestrial observations imply a total mass of ^{60}Fe in the interstellar medium dust of 5-11 $\times$ 10^{-5} $M_\odot$, which is between 10 and 1000 times more than the ^{60}Fe produced in (super)-asymptotic giant branch stars. Based on astrophysical calculations, the abundance of ^{60}Fe measured in terrestrial samples implies a distance of ~10–100 pc for the SN event (Fields et al., 2005). A subsequent study of various possible influences on the path of interstellar dust carrying the ^{60}Fe provided an improved estimate of the distance as 46 ± 8 pc (Fry et al., 2015). A different calculation based on probable trajectories of ^{60}Fe and masses of the SN progenitors suggested a value of 90 pc (Breitschwerdt et al., 2016).

In contrast to ^{60}Fe, SN explosions are not a significant source of ^{3}He to Earth. Given that the mass of SN ejecta is about 10^{-5} $M_\odot$ of ^{3}He (about 4 $\times$ 10^{51} atoms of ^{3}He), the surface density of ^{3}He spread over a sphere of 40 pc radius is ~2 $\times$ 10^{10} atoms/cm^2. Assuming this spreading happens over ~1000-year timescales, the flux will be ~2 $\times$ 10^7 atoms/cm^2/yr; realistic distances and timescales are likely longer (Fry et al., 2015), leading to a smaller flux. The SN ^{3}He will be in the gas phase, while some, if not most, of the ^{60}Fe will go into the dust. Only the dust phase penetrates the heliosphere all the way to Earth, which strongly enhances terrestrial deposition of supernova ^{60}Fe relative to any supernova ^{3}He. By comparison, solar wind-implanted ^{3}He in IDPs appears to dominate the ^{3}He flux to Earth. The predicted SN ^{3}He/^{4}He ratio is ~75 R_A (Limongi and Chieffi, 2003), significantly lower than extreme values (up to 4400 R_A) measured in ferromanganese crusts (Basu et al., 2006, 2007). There are many other details that are poorly understood, including the extent to which any ^{3}He may be implanted into dust of the SN remnant, and the extent to which cosmic rays from the SN itself, such as high-energy ^{4}He atoms, collide with the dust grains and produce fragments of ^{3}He. These latter two effects are thought to be insignificant.

The effects of a nearby SN explosion on Earth's surface and biota are topics of great interest (Benitez et al., 2002; Beech, 2011; Svensmark, 2012; Thomas et al., 2016; Melott et al., 2017; Thomas, 2018). Thomas et al. (2016) suggested that an event at ~50 pc would have only a small effect on organisms from the visible light changes, and that chemical changes such as ozone depletion would be relatively weak. However, high-energy cosmic ray penetration would dramatically increase and may cause tropospheric ionization and lightning that extends all the way to the ground surface for timescales of 1–10 kyr (Thomas et al., 2016; Melott et al., 2017). Cosmic ray muon irradiation is also estimated to increase by a factor of ~150, which would increase the radiation load on terrestrial organisms by about a factor of 10, and might lead to increases in plant damage, cancer, and DNA mutation rates. Thomas (2018) suggested the SN event(s) between 3 and 1.5 Ma could be linked to changes in species turnover near the Pliocene-Pleistocene boundary.

2.2. ^{60}Fe in Terrestrial Samples

Live ^{60}Fe, having a half-life = 2.6 Myr (Rugel et al., 2009; Wallner et al., 2015) was first reported in a terrestrial sample by Knie et al. (1999). Live ^{60}Fe has since been measured in samples of ferromanganese crusts (Knie et al. 1999, 2004), marine sediments (Fitoussi et al., 2008; Wallner et al., 2016; Wallner et al., 2020), lunar surface materials (Fimiani et al., 2016), Antarctic snow (Koll et al., 2019), and even fossilized chains of nanocrystals produced by magnetotactic bacteria in a Pacific sediment (Ludwig et al., 2016). The expected intensity of the ^{60}Fe signal in cores ELT49-53 (4310 m water depth) and ELT45-21 (4305 m water depth) from the southeast Indian Ocean off Australia (USNS Eltanin Sediment Descripions 1973, cruises 4–54; USNS Eltanin core Descriptions 1971, cores 32–45), based on the occurrence of a nearby SN event, was originally estimated by Feige et al. (2012) using the earlier analyses of ferromanganese crusts. The predictions agreed well with the eventual analyses of sediments in the 1.7–3.2 Ma interval that were carried out by Wallner et al. (2016). Sedimentation rates in the cores are low at 2–3 mm kyr^{-1} based on magnetostratigraphy and ^{26}Al and ^{10}Be (Allison and Ledbetter, 1982; Wallner et al., 2016). Based on the ^{60}Fe record in marine sediments and ferromanganese crusts from different ocean basins, the ^{60}Fe deposition peak appears to be global, it is extended in time, and it may have originated from multiple astrophysical events (Wallner et al., 2016).

The ^{60}Fe peak that began near 3.2 Ma is close to the time that Earth's temperature began to decrease during the Pliocene-Pleistocene transition. Furthermore, the age duration of ~1.5 Myr between 3.2 and 1.7 Ma is much longer than the transport time (mean value ~200 kyr) expected for ejecta from a Local Bubble SN explosion. Thus, the duration recorded in sediments appears inconsistent with a single SN event. The duration may be consistent with movement across the solar system of SN ejecta in a series of fronts formed in short succession (Wallner et al., 2016). This would require a frequency of about two SN explosions per million years.

2.3. ^{3}He and ^{60}Fe: The Galactic Cosmic Ray Hypothesis

Studies by Basu et al. (2006, 2007) and Stuart and Lee (2012) on ^{3}He in ferromanganese crusts suggested that there may be significant complications with a supernova source for the terrestrial ^{60}Fe excesses. In their analysis of the same crust that was analyzed for ^{60}Fe by Knie et al. (1999, 2004), Basu et al. (2007) showed that several of the <4 Myr old layers contained extraterrestrial helium having ^{3}He/^{4}He ratios much higher than the solar wind value (>290

R_A), in one case reaching as high as 4400 R_A. They interpreted these extreme compositions to result from incorporation of micrometeorite grains that were irradiated for hundreds of millions of years by GCRs in the interstellar medium, outside of the solar system where the flux is thought to be larger than the solar wind ^3He flux. They further suggested that the ^{60}Fe excesses were generated by reactions of GCRs on nickel-bearing minerals in iron meteorites. The $^3He/^4He$ variations in the ferromanganese crust are controlled primarily by the concentrations of ^3He. Furthermore, there appears to have been a significant change in the ^3He record at ~4 Ma. Before that time the ^3He concentration varied by about a factor of 10 and there were no $^3He/^4He$ ratios higher than the solar wind value. After 4 Ma the ^3He concentration varied by >100 and the average $^3He/^4He$ ratio was higher (after 4 Ma compared to 54 R_A before 4 Ma). Most notably, six sample layers had $^3He/^4He$ in excess of the solar wind value, ranging up to .

Basu et al. (2007) argued that such high $^3He/^4He$ ratios can only indicate the presence of particles carrying GCR-produced ^3He. However, the highest $^3He/^4He$ ratios measured in stratospheric dust grains ("cluster IDPs") range to >40× the solar wind value, or ~11600 R_A (Nier and Schlutter, 1993; Pepin et al. 2000, 2001). Such high values do remain difficult to explain by spallation production of ^3He, during the typical exposure times of particles in interplanetary space that are computed from dynamical models of particle drag. Prolonged irradiation of the particles during burial in a parent body regolith prior to their ejection as IDPs also appears unreasonable, unless the parent bodies reside in the Kuiper Belt and the dust particles are transported to the inner solar system by comets (Pepin et al. 2001). Because such a high $^3He/^4He$ signal has not been observed in any marine sediment to date, Basu et al. (2007) argued that the increase in the ferromanganese crust ^3He after 4 Ma does not result from an increase in the intensity of the cosmic dust flux to Earth, but rather to an increase in trapping efficency within the ferromanganese crust, of dense micrometeorite particles after settling through the ocean, perhaps in response to changing oceanographic conditions in the region. The Basu et al. (2007) results indicate that more work is warranted on marine sediments and crusts to evaluate how ^3He variations may shed light on the origin and time scale of ^{60}Fe variations.

2.4. Interplanetary Dust and ^3He in Marine Sediments

Cosmic dust comprises an important marine sedimentary component for some elements and isotopes, most notably Ir, Os and ^3He. The accretion rate of cosmic dust is 40×10^6 kg yr^{-1} based on measurements of hypervelocity impact craters on the Long Duration Exposure Facility satellite (Love and Brownlee 1993). This value is similar to estimates of 50-56 $\times 10^6$ kg yr^{-1} (Esser and Turekian 1988) and 30 ± 15 $\times 10^6$ kg yr^{-1} (Peucker-Ehrenbrink and Ravizza 2000) based on Os isotopes of deep sea sediments and ferromanganese deposits.

Helium in marine sediments is generally accepted to be a binary mixture of two dominant sources - extraterrestrial dust and terrigenous dust. From step heating, leaching, size fractionation magnetic separation experiments, and microscopic investigation, ^3He in the extraterrestrial component is dominantly located in silicates, Fe-Ni sulfides, magnetite and/or Fe-Ti oxides (Mukhopadhyay and Farley, 2006; Darrah and Poreda, 2012). This ^3He is preferentially concentrated in finer grained material: ≤20% occurs in grain sizes >50 μm (Mukhopadhyay and Farley, 2006). Deep sea sediments have some of the highest $^3He/^4He$ ratios on Earth, up to about 150 R_A, where R_A is the atmospheric ratio of 1.39×10^{-6} (see Farley, 2001; McGee and Mukhopadhyay, 2013 for detailed reviews). The extraterrestrial component of ^3He in such mixtures is defined as.

$[^3He]_{ET} = [^3He]_M\{(1\text{-}R_{TERR}/R_M)/(1\text{-}R_{TERR}/R_{ET})\}$where R is the $^3He/^4He$ ratio, and M, TERR and ET are the measured, terrigenous and extraterrestrial values, respectively. In most open-ocean locations, $[^3He]_{ET}$ will be >90% of the measured [^3He], because the extraterrestrial $^3He/^4He$ ratio is about 10^4 times larger than the $^3He/^4He$ ratio in crustal rocks.

The $^3He_{ET}$ record is well preserved in marine sediments on time scales of 10^7-10^8 years, and perhaps longer given evidence for its preservation in 480 Myr old limestone (Patterson et al., 1998). Changes in IDP flux associated with both asteroid breakup events in the Miocene and comet showers in the Eocene have been postulated (Farley et al., 1998, 2006; Farley, 2009), but it appears that in general the $^3He_{ET}$ accumulation rate in marine sediments has been roughly constant on million year time scales during most of the Cenozoic, leading to the concept of using $^3He_{ET}$ as a constant flux proxy.

To test for periodic variations in IDP flux, Marcantonio et al. (1995, 1996, 1999, 2001) normalized their ^3He data for young marine sediments to $^{230}Th_{excess}$ (a radioactive tracer of particle accumulation rate, having a 75 kyr half-life). When the ^3He data were normalized in this way, most of the variations in ^3He accumulation rate were removed, and the supply rate of ^3He appeared to be constant to within 30% (at ~0.8×10^{-12} cm^3 STP cm^{-2} kyr^{-1}). This flux estimate overlaps values of 0.6–1.2 $\times 10^{-12}$ cm^3 STP cm^{-2} kyr^{-1} determined for polar ice cores (Brook et al., 2000, 2009; Winckler and Fischer, 2006). Assuming that cosmic dust has [^3He] = 2×10^{-5} cm^3 STP g^{-1}, similar to values measured in stratospheric particles (Nier and Schlutter, 1990), a cosmic dust flux of ~260 tons yr^{-1} will support the observed $^3He_{ET}$. This flux estimate is ~0.5–1% of the dust flux estimated from Os isotopes (5.0–5.6 $\times 10^4$ tons yr^{-1} by Esser and Turekian, 1988; 3.0 ± 1.5 $\times 10^4$ tons yr^{-1} by Peucker-Ehrenbrink and Ravizza, 2000), with the difference attributed to differences in the size range of particles carrying the Os and ^3He inventories. This size dependence results from the fact that IDPs that are much larger than about 20 μm generally do not retain their noble gases during atmospheric entry heating and ablation (Trull, 1994; Farley et al., 1997), so most of the extraterrestrial noble gases in deep-sea sediments should be carried by particles smaller than this size.

The reproducibility of sediment measurements is generally consistent with the Farley et al. (1997) model that assumes ^3He in IDPs is a surface correlated component (McGee and Mukhopadhyay, 2013). This has been taken to mean that the $^3He_{ET}$ component is mostly located within some number of fine grains rather than in a comparatively smaller number of large grains. When attempting to accurately quantify the influence of particle variability-one needs to sample a large enough population of particles by taking a large enough sample. This leads to the concept of the Area-Time (A•T) product (Farley et al., 1997; Peucker-Ehrenbrink and Ravizza, 2000; Farley, 2001). A•T = x/MAR, where x is sample size (g) and MAR is mass accumulation rate (g-m^{-2}-yr^{-1}). The probability of missing rare, intermediate size but potentially important particles, and thereby the likelihood of underestimating the $^3He_{ET}$ flux, increases with decreasing A•T (i.e., with decreases in sample size and increases in accumulation rate). Accurately quantifying the random nature of the ET mass flux to Earth requires A•T on the order of 2.5 m^2 yr (Farley et al., 1997). In the case of the present study, a 0.2 g sediment sample from a core having a mass accumulation rate of 2 g-m^{-2}-yr^{-1} (i.e., sediment dry bulk density = 0.7 g cm^{-3}, sedimentation rate = 2.5 mm kyr^{-1}, similar to ELT49-53 in this study) will have A•T = 0.1 m^2 yr. Consequently, replicate analyses are important to accurately characterize the $^3He_{ET}$ level, as well as the need to treat outlier data with caution (Farley et al., 1997; Torfstein, 2012). Although there is commonly a problem of undersampling for the *total IDP mass* at values of A•T = 0.10 m^2

yr, the sampling for *surface correlated IDP* ^3He is not as biased (Peucker-Ehrenbrink et al., 2016). In a study of sediments near the Juan de Fuca Ridge, Middleton et al. (2020) found a 1-sigma $^3He_{ET}$ uncertainty of ~39% for 164 replicate sample pairs where the A•T product was ~0.10 m^2 yr. In a study of surface pelagic clays from the northern equatorial Pacific, Torfstein (2012) showed that $^3He_{ET}$ reproducibility was better than model predictions. He suggested that, in fact, most of the $^3He_{ET}$ is concentrated in finer particles (<2 μm), leading to a more homogeneous $^3He_{ET}$ distribution in the sediments than predicted by the surface correlated model in which most $^3He_{ET}$ is assumed to be concentrated in 5–10 μm IDP grains. In contrast, for western N Atlantic sediments McGee et al. (2010) found that >90% of the $^3He_{ET}$ was in < 20 μm grains, with roughly equal inventories in <4 μm and 4–20 μm grain sizes. With respect to the present study, A•T varies from 0.05 to 0.12 cm^2 yr. This can lead to relatively large sigma values for $^3He_{ET}$ (~60%, see Section 4.2 Results).

2.5. The Eltanin Cores

In this project we leverage the extensive ^{60}Fe analytical work by accelerator mass specrometry already carried out on the Eltanin cores. Our analytical work concentrated on ELT49-53 (located at 37.86°S, 100.03°E, water depth = 4310 m). The ELT49-53 age model is based on the ^{26}Al and ^{10}Be results of Wallner et al. (2016). The core sections investigated here (100 to 600 cm depth) are dominantly comprised of slowly accumulating foraminiferal ooze. Wallner et al. (2016) leached authigenic Fe from ~3 g of sediment taken over ~1 cm depth intervals (representing a depositional time period of ~3 kyr given the sedimentation rate of ~3 mm kyr^{-1}), following extraction methods outlined by Feige et al. (2013). Each sample contained between a few 10^3 and 10^5 atoms of ^{60}Fe; $^{60}Fe/Fe$ ratios are order of 10^{-15} in the core intervals showing ^{60}Fe excess. In the time period between 1.7 and 3.2 Ma, 288 counts of ^{60}Fe were detected (the sum total for 45 individual sediment samples taken from four different cores). Of the 7 additional samples taken from <0.2 Ma or ≥4 Ma, no ^{60}Fe was detected above the extremely low background levels (e.g., compared to the 99 "blank samples" of commercial Fe analyzed during the study that registered a total of 7 counts of ^{60}Fe).

3. Methods

3.1. Helium Isotope Measurements

Samples of 1-cm^3 size were extracted from the sediment cores using a subcore syringe Fifty-three samples were analyzed from ELT49-53 (ten in duplicate and one in triplicate), plus two samples each from ELT45-21 and ELT50-02. All sediment samples were freeze dried, and in most cases twice. Bulk sediment weighing approximately 100–250 mg was wrapped in a tin foil package and loaded into a stainless steel carousel that allowed samples to be sequentially dropped into a high temperature resistively heated vacuum furnace. Sediment was melted at >1400 °C. The gas released during heating was exposed to a stainless steel U-trap held at 77 K using liquid N_2. Water vapor and other condensed phases in this trap were pumped between sample runs through a separate conduit, which helped to maintain low background pressure in the vacuum line and not limit the sample processing time. When sample heating was completed, the gas not trapped at 77 K was processed through a series of SAES getters to remove reactive species, and the noble gases were then cryo-sorbed onto activated charcoal at 10 K. Helium was selectively released from the cryogenic trap at 45 K and admitted to the mass spectrometer. Analyses were carried out as described previously in Graham et al. (2014). Sample $^3He/^4He$ ratios and He concentrations were computed by comparison to the lab running standard HESJ (the Helium Standard of Japan, having $^3He/^4He$ = 20.4 R_A). Furnace hot blanks were routinely analyzed before and after each sample, and blank corrections were applied to the measured results. Routine blanks for ^3He and ^4He were well below 1% of the amount of helium analyzed in nearly all cases. Analytical reproducibility of ^3He and ^4He in the size range of samples was better than 1% based on replicate analyses of HESJ aliquots. Replicate analyses of samples show much larger variability, likely due to heterogeneous distribution of rare helium-rich IDPs that are not always representatively sampled (see Section 4.2).

3.2. $CaCO_3$ Content Analyses

Aliquots of dry bulk sediment from ELT49-53 were analyzed for % $CaCO_3$ with a UIC, Inc. model 5014 CO_2 coulometer coupled to an AutoMate sample preparation device controlled by LabView software. Analytical sessions allowed up to 45 analyses of samples, standards and blanks via a 45-position carousel. Method details are outlined in Morth and Backman (2011). Approximately 10–15 mg of sediment was weighed and quantitatively transferred into a 12-ml glass vial that was then tightly closed with a septum seal. Samples were acidified with 4 ml of 10% H_3PO_4 and the evolved CO_2 gas was stripped and transferred to the coulometer using ultrapure N_2 carrier gas. Analyses typically required 6–8 min to achieve a 0.15% measurement difference between successive minutes during the titration. In the latter part of the analyses, the delivery Teflon tubing and sample vial were flushed with an additional 4 ml of deionized water. The evolved CO_2 was titrated electrochemically in a glass cell comprised of a Pt cathode and Ag anode, containing a saturated KI solution and proprietary carbon indicator solution.

4. Results

4.1. Variation in $CaCO_3$ Content

The $CaCO_3$ content in ELT49-53 varies from 37.8 to 88.7% (Supplementary Data Table 1). Ten samples were analyzed in duplicate. The standard deviation of these replicate analyses was 0.76%, which is small compared to the $CaCO_3$ content variation of nearly 50%. Some of the variability in sample reproducibility may represent sample heterogeneity, but most of it is related to uncertainties in sample weighing; e.g., a standard deviation of 0.76% for our 10 replicates translates to an error of only 0.08 mg for 10 mg aliquots of sediment.

4.2. ^3He and ^4He Concentrations

Helium concentration results for 69 sample analyses are presented in Supplementary Data Table 1. The bulk sediment ^3He concentration varies by a factor of 86, from 1.4×10^{-12} to 1.2×10^{-10} cm^3 STP/g. The distribution of [^3He] is highly skewed; excluding the four highest outliers reduces the variation to a factor of 11 (maximum [^3He] = 1.6×10^{-11} cm^3 STP/g). Bulk ^4He concentrations vary by a factor of 10, from 1.2×10^{-7} to 1.4×10^{-6} cm^3 STP/g. Uncertainties in ^3He and ^4He for samples are larger than the analytical uncertainty associated with standard gas analyses (<1%) due to heterogeneity in the distribution of carrier phases such as IDPs and lithogenic material. Reproducibility for 11 samples (ten duplicates and one triplicate) was ±17.7% (1-standard deviation) for bulk sediment [^4He], and ±59.8% for bulk [^3He]. This variability for ^3He is somewhat larger than what would be expected for a surface correlated tracer of IDPs (Farley et al., 1997; Patterson and

Farley, 1998) given the range of 0.05–0.12 m^2 yr for the Area*Time product in the present study. This higher variability is probably related to the small number of replicate analyses in our study.

There is an anti-correlation between ^4He and %$CaCO_3$ (Fig. 1), having a correlation coefficient r = −0.95, and intercept (at 0% carbonate) b = 2.3 × 10^{-6} cm^3 STP/g. This strong anti-correlation represents a classic binary mixing/carbonate dilution trend in which the non-carbonate fraction effectively carries all of the sedimentary helium. The co-variation between ^3He and %$CaCO_3$ is not as strong as for ^4He. However, excluding 6 samples that have [^3He] above 1.25 × 10^{-11} cm^3 STP/g gives an overall correlation of r = −0.78, a clear indication for a significant dilution of the ^3He signal by $CaCO_3$.

The helium concentration in the non-carbonate sediment fraction is given by

$$[He]_{nc} = [He]_{bulk}/(1 - \%CaCO_3/100)$$

The [^3He]$_{nc}$ varies by a factor of 88, from 5 × 10^{-12} to 4.4 × 10^{-10} cm^3 STP/g. Excluding the four highest outliers reduces the variation to a factor of 7 (maximum [^3He]$_{nc}$ = 3.5 × 10^{-11} cm^3 STP/g). ^4He concentrations in the non-carbonate fraction vary by a factor of 3.7, from 9.2 × 10^{-7} to 3.4 × 10^{-6} cm^3 STP/g.

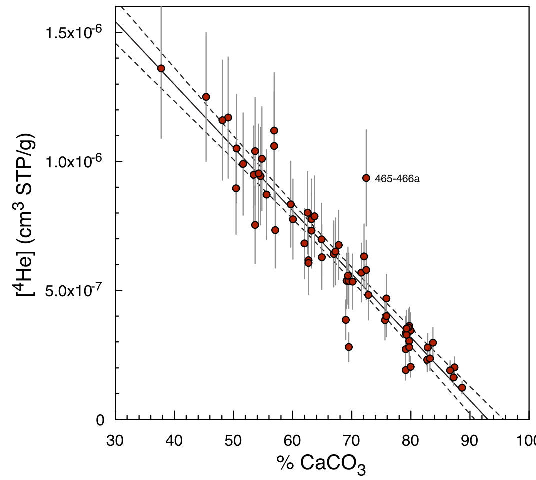

Fig. 1. Dry bulk sediment ^4He (cm^3 STP/g) vs % $CaCO_3$ for ELT49-53. Uncertainties shown for ^4He are ± 20%, consistent with the reproducibility of replicate samples in this study. Analytical uncertainties in ^4He associated with instrumental analysis are <1%. The linear correlation is described by y = −2.45 × 10^{-8}x + 2.28 × 10^{-6}; r = −0.945. The dashed line shows 95% confidence limits on the regression.

5. Discussion

The effective absence of ^4He in the carbonate fraction of marine sediments (Fig. 1) has been recognized before, and attributed to efficient ejection of *in situ* generated alpha-particles from the relatively fine-grained $CaCO_3$, as well as to diffusive loss (Patterson and Farley, 1998). The terrestrial helium component in marine sediments is therefore dominated by the terrigenous fraction.

Downcore variations in ELT49-53 are shown in Fig. 2. The strong anti-correlation between $CaCO_3$ content and bulk [^4He] described in Fig. 1 is apparent. Variations in non-carbonate [^3He] and [^4He], while significant at factors of 7 (excluding the four highest ^3He outliers) and 3.7, respectively, are low compared to the bulk sediment concentrations (factors of 11 and 10, respectively) due to the ~50% variation in $CaCO_3$ content. The ELT49-53 sediments contain a minor, but non-quantified opal component. Rare diatoms were present during inspection of some sample residues remaining from the carbonate analyses, but they appear to be a minor component of the non-carbonate fraction. In this study, we consider the non-carbonate helium concentration to be equivalent to the helium concentration in the terrigenous fraction of each sample.

In all cases, the [^3He]$_{ET}$ for ELT49-53 samples represents >99% of the measured [^3He] (assuming R_{TERR} = 4 × 10^{-8} and R_{ET} = 2.8 × 10^{-4}; see further discussion of the chosen end-member values in Section 5.3). There are some "spikes" in the $^3He_{ET}$ record (Fig. 2). These could indicate the presence of a condensed stratigraphic horizon caused by intervals of "non-deposition", but they cannot be due to the presence of a hiatus because this process would remove the ^3He-enriched IDPs along with other sedimentary components. These anomalous "spikes" might also respresent the rare presence of ^3He-rich micrometorites or cluster IDPs. The most extreme sample in the piston core record (ELT49-53, 465-466a) has $^3He/^4He$ = 94 R_A and the highest ^3He concentration (by an order of magnitude; 1.2 × 10^{-10} cm^3 STP/g). It occurs at 465 cm depth (age of 2.99 Ma, close to the initial increase of ^{60}Fe). We were not able to replicate this $^3He/^4He$ result through additional analysis of this sample, suggesting that the anomalous composition may result from the so called "nugget" effect. Poor reproducibility of a small number of sediment core samples has been observed in some earlier studies. Torfstein (2012) showed that in the northern equatorial Pacific, >90% of the extraterrestrial ^3He was concentrated in particles below 20 um in diameter. He further suggested that a small number of his anomalously high ^3He samples were due to the presence of a few very helium-rich particles below 20 μm in size. The size of the ^3He anomaly in ELT49-53 sample 465–466a is 1.4 × 10^{-11} cm^3 STP (i.e., 1.2 × 10^{-10} cm^3 STP/g ^3He in 120 mg; Supplementary Data Table 1). If all the measured ^3He was from a single IDP particle that was 20 μm diameter (having density = 2 g/cm^3), it would correspond to [^3He] = 1.7 × 10^{-3} cm^3 STP/g in the IDP. This is a factor of 335 higher than the median value (5 × 10^{-6} cm^3 STP/g) measured in stratospheric particles by Nier and Schlutter (1990), and a factor 29 higher than the highest value they measured (5.8 × 10^{-5} cm^3 STP/g). The 465-466a sample also has the highest ^4He in our data set, further standing out because it lies well above the [^4He]-$CaCO_3$ anti-correlation seen in Fig. 1. These observations support the argument of Torfstein (2012) that helium-rich particles having elevated levels of both ^3He and ^4He are present in some IDP samples.

5.1. Absence of ^3He - ^{60}Fe Co-variation: Circumstantial Evidence for the Supernova Hypothesis

The SN hypothesis states that terrestrial ^{60}Fe is derived from supernova input. Following this hypothesis, we would expect to see no covariation in the measured levels of terrestrial $^3He_{ET}$ and ^{60}Fe if $^3He_{ET}$ is derived from IDPs. (A covariation might also be absent if there were different host phases for ^3He and ^{60}Fe, or different amounts of post-depositional loss). The GCR hypothesis states that terrestrial ^{60}Fe is derived from micrometeorites through reactions of GCRs on grains that were irradiated for hundreds of millions of years in the interstellar medium. The GCR ^3He production rate in interstellar space is expected to be at least four times larger than ^3He produced by the solar wind (Reedy, 1987), so one might expect to see a positive correlation in the measured levels of terrestrial $^3He_{ET}$ and ^{60}Fe if they are derived from GCR-irradiated micrometeorites. However, the absence of such a correlation does not allow a firm rejection of the GCR hypothesis, and should be viewed as circumstantial evidence supporting the SN hypothesis.

Fig. 3 shows the $^{60}Fe/Fe$ ratio vs the concentrations of ^3He and ^4He in the non-carbonate fraction of ELT49-53 sediment. The data for 30 samples are plotted in each case (Fig. 3a, b), and one sample (246–247 cm depth) has been excluded due to its very large error in the $^{60}Fe/Fe$ ratio. There is no trend of $^{60}Fe/Fe$ with ^3He when all

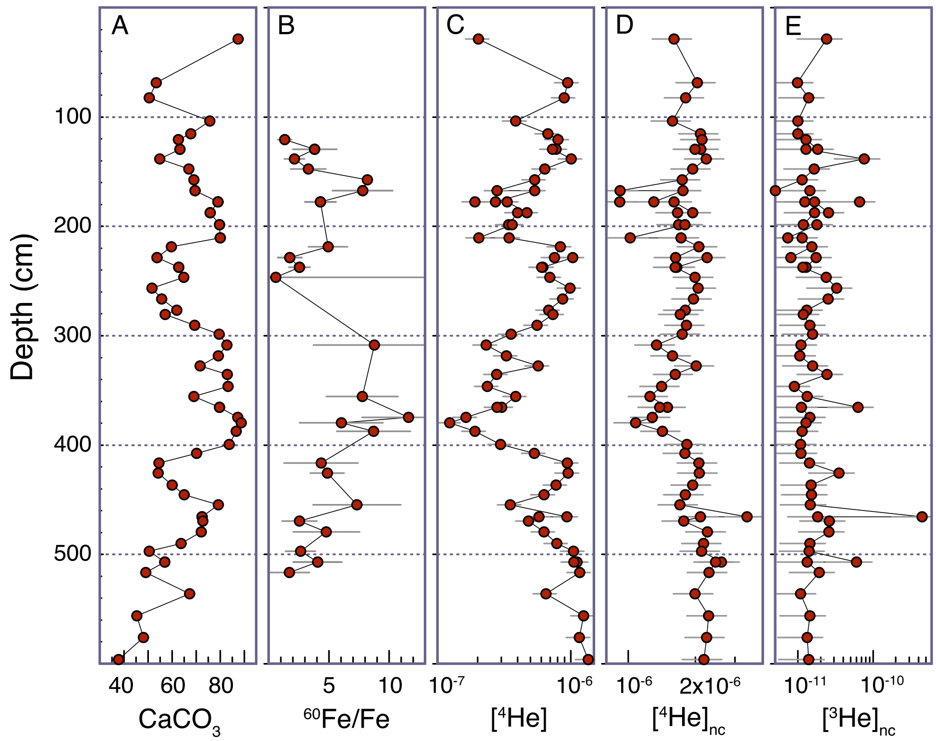

Fig. 2. Downcore variations in (A) % $CaCO_3$, (B) decay-corrected $^{60}Fe/Fe$ (10^{-15} at/at), from Wallner et al. (2016), (C) bulk [^4He] (cm^3 STP/g), (D) non-carbonate [^4He] (cm^3 STP/g), E) non-carbonate [^3He] (cm^3 STP/g). Uncertainties in ^3He and ^4He are ± 60% and ± 20%, respectively, consistent with the reproducibility of replicate samples in this study.

30 sample pairs are included (correlation coefficient R = −0.24), nor when the highest four ^3He data points are excluded (R = −0.28). There does seem to be a negative trend of $^{60}Fe/Fe$ with ^4He (linear regression R = −0.54). The analytical errors on ^{60}Fe are large and so the question arises as to the likelihood that we could miss a true correlation in this data set. To further evaluate that possibility we performed several Monte Carlo simulations.

In the simulations, $[^3He]_{nc}$, $[^4He]_{nc}$, and $^{60}Fe/Fe$ were varied randomly within specified limits. In the case of $^{60}Fe/Fe$, the selected limit was the 1-sigma uncertainty in the ratio (Supplementary Data Table 1). For the cases of ^3He and ^4He, the concentrations were assigned uncertainties of ±60% and ±20%, respectively, consistent with reproducibility for the sample analyses (Section 4.2). Ten thousand iterations using a Monte Carlo approach showed that 1.4% and 27.5% of the ^3He and ^4He trials, respectively, fall above the absolute value of the critical correlation coefficent for 95% confidence ($|R_{crit}|$, which equals 0.361 when n = 30; Fig. 3c, d). A choice of a smaller uncertainty for the He concentrations (e.g., 30% and 10% for ^3He and ^4He, respectively) leads to a larger percentage of cases greater than $|R_{crit}|$ for ^4He (48.6%) but no significant change for ^3He (1.1%). A choice of a larger uncertainty for ^3He and ^4He concentration has the opposite effect for ^4He but no effect for ^3He; for example, a 30% uncertainty in ^4He and 75% uncertainty in ^3He produces 18.8% greater than |Rcrit| for ^4He but only 1.3% for ^3He.

The absence of a positive co-variation between the measured $[^3He]_{nc}$ and decay-corrected $^{60}Fe/Fe$ (Fig. 3a, c) is circumstantial support for the SN hypothesis. It is circumstantial because the extent to which the GCR flux will produce correlated ^3He and ^{60}Fe levels in micrometeorite grains is not well known. One might expect that the amount of GCR radiation required to produce measurable ^{60}Fe throughout the core interval would generate a measurably higher amount of ^3He throughout the same interval, but this is not established. It also is not known whether a substantial amount of the total ^3He in the sediments would be associated with ^{60}Fe-rich particles compared to the background IDPs that are present. This means that an enhanced flux of ^{60}Fe- and metal-rich micrometeorites might occur without a significant increase in overall cosmic dust flux, possibly leading to no ^3He-^{60}Fe covariation. These scenarios need better evaluation in the future.

Although our ^3He-^{60}Fe results may provide only circumstantial evidence in favor of the SN hypothesis, several other observations are relevant in the debate. First, Wallner et al. (2016) showed that the observed influx of ^{60}Fe is ~400× higher than expected from a constant influx of IDPs where ^{60}Fe is formed by nuclear reactions. Second, the ^3He levels in the ferromanganese crust studied by Basu et al. (2007) are not simply coupled to its ^{60}Fe-rich layers. Third, Fimiani et al. (2016) showed that ^{60}Fe in lunar soils appears to have a supernova origin because its $^{60}Fe/^{53}Mn$ activity ratio is much higher than the ratio in meteorites, where both nuclides are of cosmogenic origin.

We speculate that the tendency for a negative covariation between $[^4He]_{nc}$ and $^{60}Fe/Fe$ (Fig. 3b, d) may arise from complexities in the marine geochemical cycling of Fe. ^4He is a proxy for lithogenic input to marine sediments (Patterson et al., 1999; Serno et al., 2014; Middleton et al., 2018) while the main sources of Fe include rivers, atmospheric dust, hydrothermal vents, and the resuspension of shelf and deep sea sediments (Bergquist, 2004; Raiswell and Canfield, 2012; Conway and John, 2014). Fe is also highly reactive and it has a low solubility in seawater, leading to a short residence time and a rapidly decreasing concentration away from its source areas. High sedimentary ^4He flux therefore suggests higher dust flux, which brings more total Fe to the surface ocean and drives more total Fe dissolved in the water column, leading to overall lower $^{60}Fe/Fe$ ratios. It is thought that the main sources of dissolved Fe to the Indian Ocean are atmospheric dust and rivers, plus resuspension of material from the continental shelves (Chinni et al., 2019). The primary removal mechanism of Fe is through burial of sinking biological material plus Fe

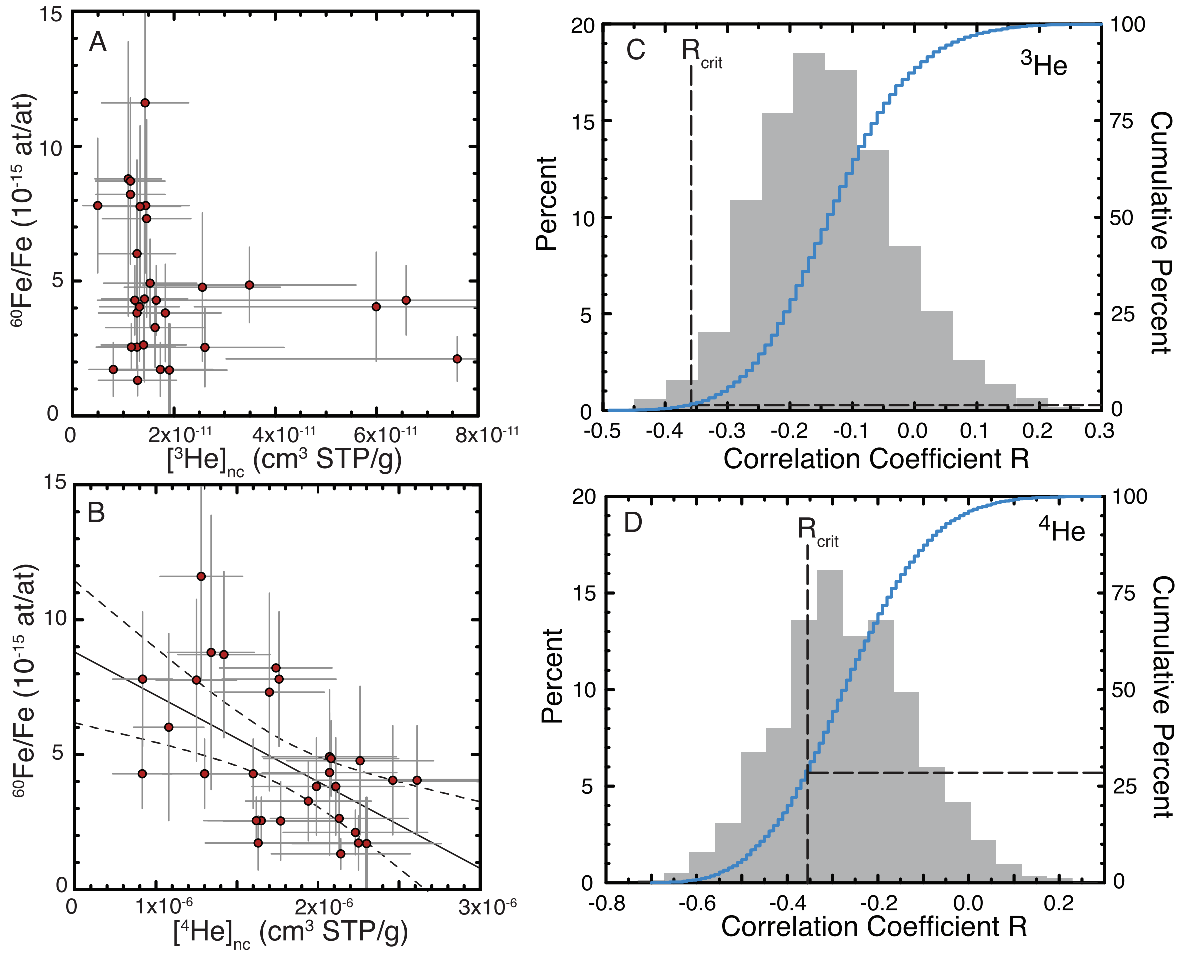

Fig. 3. (A) Non-carbonate [^{3}He] (cm^3 STP/g) and (B) non-carbonate [^{4}He] (cm^3 STP/g) vs decay-corrected ^{60}Fe/Fe (10^{-15} at/at). The ^{60}Fe data are from Wallner et al. (2016). The simple linear regression shown in panel B has a correlation coefficient R = –0.537, and the 95% confidence limit on the fit is shown by the dashed envelope. Relative histograms for Monte Carlo simulations of the He-^{60}Fe covariations are shown in panel C (^{3}He) and panel D (^{4}He). The simulations were carried out for 10,000 trials of paired He – ^{60}Fe/Fe data points (n = 30) chosen randomly by having the uncertainties shown for ^{60}Fe/Fe (see Supplementary Data Table 1), and assuming 60% and 20% uncertainties in the concentrations of ^{3}He and ^{4}He respectively, consistent with the reproducibility of replicate samples in this study. The 95% confidence level is given by $|R_{crit}| > 0.361$ when the number of samples n = 30. The blue curves show the cumulative probability in each case varying from 0 to 100%. Based on these Monte Carlo results, the probability of any correlation between ^{3}He and ^{60}Fe/Fe appears to be <2%. In contrast, there is a tendency for ~28% of the trials for ^{4}He and ^{60}Fe/Fe to show a significant negative correlation for the case shown here. See the text for further discussion.

scavenged onto sinking particles. If the supply flux of Fe varies through time in relation to climatic conditions (e.g., Winckler et al., 2008; Thöle et al., 2019) due to changes in continental aridity, wind direction or intensity, it is plausible that the supply of terrigenous ^{4}He and total Fe would co-vary.

5.2. ^{3}He Accumulation Rate and IDP Flux

Mass accumulation rates may be estimated from the new ^{3}He analyses in the ^{60}Fe-rich age interval assuming a known $^3He_{ET}$ flux. Alternatively, the ^{3}He accumulation rate may be estimated from the measured [^{3}He] and the sediment deposition age based on the downcore ^{26}Al and ^{10}Be records of Wallner et al. (2016). The accumulation rate of ^{3}He in ELT49-53 sediments is effectively equivalent to the IDP ^{3}He flux (F_{IDP}). Following the approach of Winckler et al. (2004) this flux (F_{IDP}) is computed as

$$F_{IDP} = [^3He](MAR)$$

where [^{3}He] = measured ^{3}He concentration in dry bulk sediment (cm^3 STP/g), and MAR = mass accumulation rate (g/cm^2/ky). The MAR is given by

$$MAR\ (g/cm^2/ky) = (DBD)(LSR)$$

where LSR = linear sedimentation rate (cm/ky) and DBD = dry bulk density (g/cm^3). LSR is computed for each sample from the relation

$$LSR_i = (z_{i+1} - z_{i-1})/(t_{i+1} - t_{i-1})$$

where i represents the depth of interest, z is depth in the core (cm) and t is its ^{10}Be or ^{26}Al age (kyr). Dry bulk densities for Eltanin sediments from the SE Indian Ocean follow the empirical relationship (Clemens et al., 1987)

$$DBD = 3.104 \times 10^{-4}(\%\,CaCO_3)^2 + 2.176 \times 10^{-3}(\%\,CaCO_3) + 0.430$$

There are a total of 54 individual determinations of the ^{3}He accumulation rate between 3.2 and 1.7 Ma in core ELT49-53, including replicate analyses (Supplementary Data Table 1). The central tendency of the data is better estimated from the median than the arithmetic mean when there is a large variance in the data set, because the median de-emphasizes the rare and anomalously high He concentrations. The median ^{3}He concentration for bulk sediments throughout core ELT49-53 (n = 65) is 4.67 × 10^{-12} cm^3 STP/g. The median ^{3}He flux (n = 54) is 0.88 ± 0.26 × 10^{-12} cm^3 STP/cm^2/kyr. The uncertainty in this flux estimate was computed from the median of the absolute deviations of the individual flux estimates from the median flux value (Winckler et al., 2004). Similarly, the median ^{4}He accumulation rate is 0.108 ± 0.036 × 10^{-6} cm^3 STP/cm^2/kyr. The ^{3}He/^{4}He accumulation ratio throughout the core (n = 65) is 7.87 ± 1.56 × 10^{-6} (5.7 ± 1.1 R_A). Temporal changes in $CaCO_3$, and in the accumulation rates of ^{4}He, ^{3}He, and ^{60}Fe rate are shown in Fig. 4.

$^3He_{ET}$ fluxes have previously been estimated from ice cores to be ~0.8 × 10^{-12} cm^3 STP ^{3}He/cm^2/kyr (Brook et al. 2000, 2009; Winckler and Fischer, 2006). Estimates from sediment cores throughout the ocean basins are similar to this value (Farley, 1995; Marcantonio et al. 1995, 1996, 1998, 1999, 2001; Patterson and Farley, 1998; Higgins et al., 2002; Winckler et al., 2004: Torfstein, 2012). The flux appears to be relatively uniform (±50%) at ~1 × 10^{-12} cm^3 STP ^{3}He/cm^2/kyr over a large range of timescales, from years to millions of years (Farley et al., 2021). Significantly, the new record of similar $^3He_{ET}$ flux from ELT 49–53 spans the time range from ~3.2–1.5 Ma, during the climatic transition from Pliocene to Pleistocene.

The similarity of the estimated ^{3}He flux between 1.7 and 3.2 Ma in ELT49-53 with the ^{230}Th-normalized ^{3}He flux in late Pleistocene cores (e.g., Marcantonio et al., 1995, 1996; Higgins et al., 2002; Winckler et al. 2004) is an interesting result, and perhaps a bit surprising given the evidence for lateral sediment focusing in the ELT49-53 area. This might be related to aggregation of fine grains, leading to less fractionation of 10–20 μm particles relative to smaller grains during sediment advection (McGee et al., 2010). In detail, the ELT49-53 $^3He_{ET}$ flux record shows one time period spanning ~70 kyr, from ~2.18 to ~2.25 Ma, when the $^3He_{ET}$ flux may have been notably elevated. This is seen in Fig. 4A as a local maximum comprised of three different samples. The highest value in this time period is 2.8 × 10^{-12} cm^3 STP/cm^2/ky, three times the median estimate for the rest of the core.

The median ^{60}Fe accumulation rate is 1.85 ± 0.5 × 10^4 at/cm^2/kyr. Some excursions to higher values appear near 2.7 and 2.95 Ma and 2.1–1.8 Ma. There are very large uncertainties however, and the excursions only occur in isolated samples. In addition, the sampling of the ^{60}Fe record is still very sparse (e.g., there is only one sample analyzed between 2.65 and 2.15 Ma). Additional and more precise (larger sample?) ^{60}Fe analyses are needed to test whether more than a single SN event is present in the record.

5.3. Provenance of Terrigenous Material in the SE Indian Ocean

The sources of terrigenous dust to the ELT49-53 deposition site in the eastern Indian Ocean are not well characterized. Abundance contours for quartz grains in surface sediments to the south and west of the Australian continental margin (see Kolla and Biscaye, 1977) suggest that Australia may be a predominant source of terrigenous material. Piketh et al. (2000) showed that eolian transport of fine dust can also occur over long distance from southern Africa to the central southern Indian Ocean, along a pathway that trends towards Australia and New Zealand. Marcantonio et al. (1999) used He, Th and Os isotopes in an equatorial Indian Ocean core (at 6°S and 89°E, which is considerably northwest of our study area) to investigate variability over the last 200 kyr. After a correction for the amount of extraterrestrial component using ^{3}He, the Os isotopes appear to fingerprint Himalayan crustal and Indonesian ultramafic rocks as primary dust sources in that region. These studies are not located in our region of study and they differ in their time ranges, but they do seem to indicate that different sources of terrigenous material may have impacted the eastern Indian Ocean since 3.2 Ma. An added complication for the EL 49–53 site is that the abyssal plain in this region can receive terrigenous material scoured by bottom currents adjacent to the Australian continental margin (Allison and Ledbetter, 1982).

The binary mixing diagram between IDPs and terrestrial material (Fig. 5) developed by Marcantonio et al. (1998) utilizes the measured ^{3}He/^{4}He ratio vs measured [^{3}He]. The IDP end-member can be constrained by measurements of stratospheric particles (Nier and Schlutter 1990, 1993). A good choice is ^{3}He/^{4}He = 2.8 × 10^{-4} (200 R_A) and [^{3}He] = 2 × 10^{-5} ccSTP/g. The dispersion in the ELT49-53 sediment data on this diagram can be explained as lying between two mixing curves having a narrow range of terrestrial ^{3}He/^{4}He = 2 × 10^{-8} to 4 × 10^{-8} (and having [^{3}He] = 10^{-14} and 10^{-13} cm^3 STP/g, respectively). The higher value for [^{3}He] is similar to the value expected from the carbonate dilution diagram (Fig. 1). That is, if $[^4He]_{nc}$ = 2.3 × 10^{-6} cm^3 STP/g (constrained from Fig. 1) then $[^3He]_{nc}$ = 9.2 × 10^{-14} cm^3 STP/g, similar to the terrigenous end-member concentration of 1 × 10^{-14} cm^3 STP/g for the ^{3}He/^{4}He = 4 × 10^{-8} model curve (Fig. 5). For the ^{3}He/^{4}He = 2 × 10^{-8} model curve, the requisite $[^3He]_{nc}$ = 4.6 × 10^{-14} cm^3 STP/g when $[^4He]_{nc}$ = 2.3 × 10^{-6} cm^3 STP/g. The difference from the model curve end-member [^{3}He] in this case may indicate some heterogeneity in the terrigenous end-member (see below).

Although $[^4He]_{nc}$ for the terrigenous end-member appears to be reasonably well-defined, its value of 2.3 × 10^{-6} cm^3 STP/g should probably be viewed as an effective value and not one that represents an inherent source characteristic. For a typical [U] = 0.9 ppm in average upper continental crust and Th/U = 3.5 (Hofmann, 1988), this amount of ^{4}He implies an "age" of only 12 Ma. This is much younger than potential terrigenous sources to the southeastern Indian Ocean, probably because large amounts of He were lost from such fine-grained material prior to its deposition. The terrigenous material at the ELT49-53 site could also be a mixture of two (or more) sources. In this case, the range for the terrigenous ^{3}He/^{4}He of 2-4 × 10^{-8} may indicate that the lithological constitution of the mixture varied, but only slightly. This situation was described by Torfstein (2012) for North Pacific surface sediments, in which the mixture there consists of ~70% loess from the Asian continent and ~30% of "low [^{3}He]" volcanic material, perhaps related to weathering of basalt terrains.

Fig. 5 shows two possible mixing curves that pass through the requisite terrestrial end-members (shown by stars). The curves were constructed for mixing between a hypothetical volcanic source having mantle ^{3}He/^{4}He (10^{-5}), and two different detrital sources, one being a "very low ^{3}He/^{4}He" and the other being an "low ^{3}He/^{4}He" material. For these hypothetical examples, the volcanic lithology would comprise 60% and >90%, respectively, of the terrestrial composite found in ELT49-53 sediments. The choices for volcanic [^{3}He] in this model may be overestimates, because they correspond to He concentrations that are commonly observed trapped in melt inclusions within igneous minerals such as olivine and pyroxene. This trapped helium should be extensively lost during chemical and physical weathering, as the initially mm-size mineral grains are reduced to the size of detrital grains. Somewhat surprisingly though, some continental materials (e.g., from Patagonia) seem to have such high [^{3}He] values (McGee et al., 2016). Although there is some uncertainty in characterizing the lithologic makeup of the terrigenous end-member in the ELT49-53 region, the most notable observation is that fine grained (<5 μm) material from Australia and China (McGee et al., 2016) form a near continuum with the ELT49-53 sediments on Fig. 5. This suggests that the terrigenous component in this region of the southeastern Indian Ocean may be comprised largely of detrital material from the interior of Australia, but more work is needed to establish such a connection.

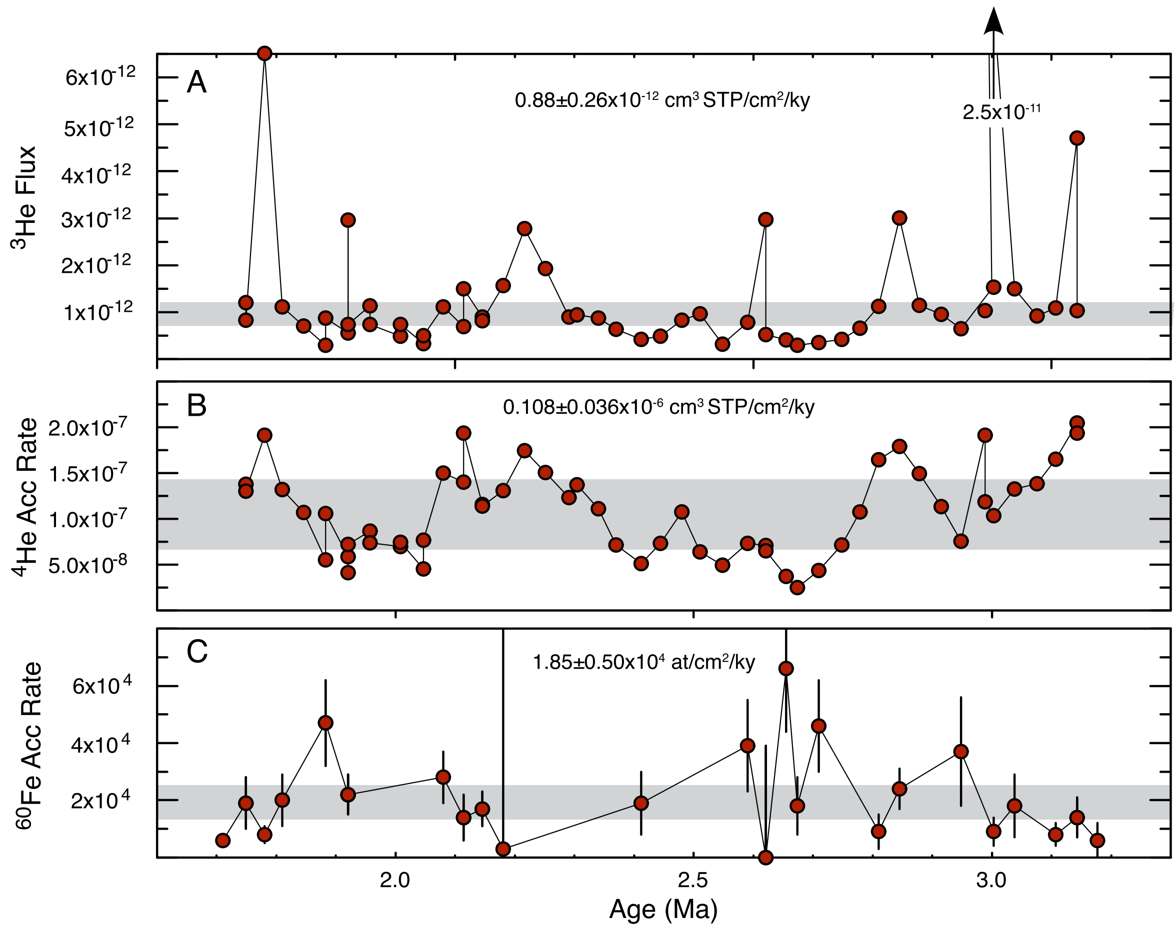

Fig. 4. Temporal variations in piston core ELT49-53. The chronology is based on ^{10}Be and ^{26}Al ages from Wallner et al. (2016). (A) ^{3}He accumulation rate (cm^3 STP/g/kyr), (B) ^{4}He accumulation rate (cm^3 STP/g/kyr), (C) ^{60}Fe accumulation rate (10^4 at/cm^2/kyr) reported by Wallner et al. 2016). Grey bands outline the median flux values and their estimated uncertainties as reported in each panel.

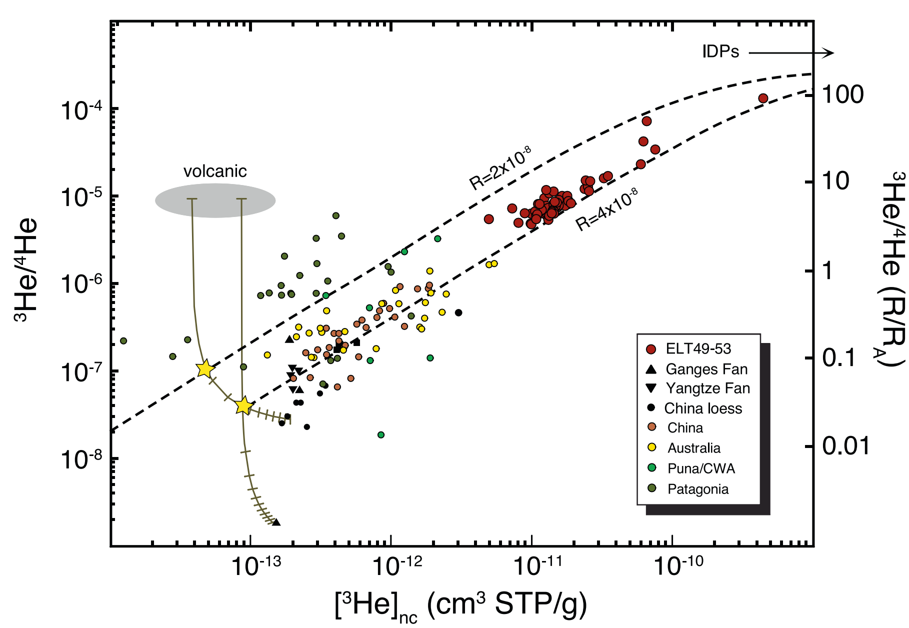

Fig. 5. $^{3}He/^{4}He$ vs non-carbonate [^{3}He] for ELT49-53 (red circles). Continental detrital data are from Marcantonio et al. (1998) and McGee et al. (2016). Binary mixing curves between IDPs and terrigenous material are shown by dashed lines, for two different terrestrial end-member $^{3}He/^{4}He$ ratios (2×10^{-8} and 4×10^{-8}). The IDP end-member has $^{3}He/^{4}He = 2.8 \times 10^{-4}$ and [^{3}He] = 2×10^{-5} cm^3 STP/g. Stars show the corresponding $[^{3}He]_{nc}$ for each mixing curve that is consistent with $[^{4}He]_{nc}$ (2.3×10^{-6} ccSTP/g) deduced from the anti-correlation between bulk [^{4}He] and %$CaCO_3$ (see Fig. 1). Two hypothetical model curves for the composition of the terrestrial component are shown, with tick marks denoting 10% fractions in each mixture. See text for discussion.

6. Conclusions

There is no evidence for a correlation between ^{3}He and ^{60}Fe in sediments from piston core ELT49-53 in the southeastern Indian Ocean. The absence of a correlation provides circumstantial evidence for the supernova hypothesis. Additional and more precise ^{60}Fe analyses are needed to firmly exclude the possibility of a ^{3}He-^{60}Fe covariation. The current ^{3}He sampling interval of ~35 kyr and such additional ^{60}Fe analyses might help discern if multiple SN or GCR events are present in the study record.

^{3}He in the sediments appears to be dominated by the presence of interplanetary dust particles (IDPs). The $^{3}He_{ET}$ flux between 3.2 and 1.7 Ma was $\sim 0.88 \pm 0.26 \times 10^{-12}$ cm^{3} STP/cm^{2}/kyr, similar to estimates from other marine sedimentary sections and ice cores that span both shorter and longer durations. Although the terrigenous component has not been uniquely identified at the core deposition site, its helium isotope characteristics resemble fine-grained (<5 μm) detrital material from the interior of Australia.

Data availability

Data are available as Supplementary Table S1

Declaration of Competing Interest

The authors declare that they have no known competing financial interests or personal relationships that could have appeared to influence the work reported in this paper.

Acknowledgments

We thank Brian Haley, Brian Fields, Ed Brook, Adam Kent, and Alan Mix for helpful discussions. Adam Kent developed the Monte Carlo tests of the ^{60}Fe-He co-variations. We thank Mitch Lyle and Annette Olivarez Lyle for developing the capability to measure sediment $CaCO_3$ contents, and for guidance and help in all aspects of the measurements. We also thank Val Stanley and the OSU Marine & Geology Repository for sampling help and access to the Eltanin cores. Two anonymous reviewers provided valuable and constructive reviews that significantly helped improve the manuscript. This study was supported by the Marine Geology & Geophysics program at NSF (OCE18-36083).

Appendix A. Supplementary material

Supplementary material to this article can be found online at https://doi.org/10.1016/j.gca.2022.09.016.

References

Allison, E., Ledbetter, M.T., 1982. Timing of bottom-water scour recorded by sedimentological parameters in the South Australian Basin. Marine Geol. 46, 131–147.
Basu, S., Stuart, F.M., Schnabel, C., Klemm, V., 2007. Galactic-cosmic-ray-produced ^{3}He in a ferromanganese crust: any supernova ^{60}Fe excess on Earth? Phys. Rev. Lett. 98, 141103-141101–141103-141106.
Basu, S., Stuart, F.M., Klemm, V., Korschinek, G., Knie, K., Hein, J.R., 2006. Helium isotopes in ferromanganese crusts from the central Pacific Ocean. Geochim. Cosmochim. Acta 70, 3996–4006.
Beech, M., 2011. The past, present and future supernova threat to Earth's biosphere. Astrophys. Space Sci. 336, 287–302.
Benitez, N., Maiz-Appleaniz, J., Canellas, M., 2002. Evidence for nearby supernova explosions. Phys. Rev. Lett. 88, 1–4.
Bergquist, B.A., 2004. The marine geochemistry of iron and iron isotopes. Ph.D. thesis, MIT-WHOI Joint Program in Oceanography. Massachusetts Institute of Technology, p. 233 pp.
Breitschwerdt, D., Feige, J., Schulreich, M.M., de Avillez, M.A., Dettbarn, C., Fuchs, B., 2016. The locations of recent supernovae near the Sun from modelling ^{60}Fe transport. Nature 532, 73–76.
Brook, E.J., Kurz, M.D., Curtice, J., 2000. Accretion of interplanetary dust in polar ice. Geophys. Res. Lett. 27, 2145–2148.
Brook, E.J., Kurz, M., Curtice, J., 2009. Flux and size fractionation of ^{3}He in interplanetary dust from Antarctic ice core samples. Earth Planet. Sci. Lett. 286, 565–569.
Chinni, V., Singh, S.K., Bhushan, R., Rengarajan, R., Sarma, V.V.S.S., 2019. Spatial variability in dissolved iron concentrations in the marginal and open waters of the Indian Ocean. Mar. Chem. 208, 11–28.
Clemens, S.C., Prell, W.L., Howard, W.R., 1987. Retrospective dry bulk density estimates from Southeast Inidain Ocean sediments - comparison of water loss and chloride-ion methods. Mar. Geol. 76, 57–69.
Conway, T.M., John, S.G., 2014. Quantification of dissolved iron sources to the North Atlantic Ocean. Nature 511, 212–220.
Darrah, T.H., Poreda, R.J., 2012. Evaluating the accretion of meteoritic debris and interplanetary dust particles in the GPC-3 sediment core using noble gas and mineralogical tracers. Geochim. Cosmochim. Acta 84, 329–352.
Ellis, J., Fields, B.D., Schramm, D.N., 1996. Geological isotope anomalies and signatures of nearby supernovae. Astrophys. J. 470, 1227–1236.
Esser, B.K., Turekian, K.K., 1988. Accretion rate of extraterrestrial particles determined from osmium isotope systematics of Pacific pelagic clay and manganese nodules. Geochim. Cosmochim. Acta 52, 1383–1388.
Farley, K.A., 1995. Cenozoic variations in the flux of interplanetary dust recorded by ^{3}He in a deep sea sediment. Nature 376, 153–156.
Farley, K.A., 2009. Late Eocene and late Miocene cosmic dust events: Comet showers, asteroid collisions, or lunar impacts? In: Koeberl, C, Montinari, A (Eds.), The Late Eocene Earth—Hothouse, Icehouse, and Impacts: GSA Special Paper 452. Geological Society of America, pp. 27–35.
Farley, K.A., Love, S.G., Patterson, D.B., 1997. Atmospheric entry heating and helium retentivity of interplanetary dust particles. Geochim. Cosmochim. Acta 61, 2309–2316.
Farley, K.A., Montanari, A., Shoemaker, E.M., Shoemaker, C.S., 1998. Geochemical evidence for a comet shower in the late Eocene. Science 280, 1250–1253.
Farley, K.A., Taylor, S., Treffkorn, J., Lever, J.H., Gow, A.L., 2021. ^{3}He flux obtained from South Pole air and snow-ice and its connection to interplanetary dust particles. Meteoritics & Planet. Sci. 56, 1988–2001.
Farley, K.A., 2001. Extraterrestrial helium in seafloor sediments: identification, characteristics, and accretion rate over geologic time. In: Peucker-Ehrenbrink B., Schmitz B. (Eds.), Accretion of Extraterrestrial Matter Throughout Earth's History, pp. 179–204.
Farley, K.A., Vokrouhlicky, D., Bottke, W.F., Nesvorny, D., 2006. A late Miocene dust shower from the break-up of an asteroid in the main belt. Nature 439, 295–297.
Feige, J., Wallner, A., Winkler, S.R., Merchel, S., Fifield, L.K., Korschinek, G., Rugel, G., Breitschwerdt, D., 2012. The search for supernova-produced radionuclides in terrestrial deep-sea archives. Publications Astron. Soc. Austr. 29, 109–114.
Feige, J., Wallner, A., Fifield, L.K., Korschinek, G., Merchel, S., Rugel, G., Steier, P., Winkler, S.R., Golser, R., 2013. AMS measurements of cosmogenic and supernova-ejected radionuclides in deep-sea sediment cores. EPJ Web Conf. 63, 5 pp.
Fields, B.D., Ellis, J., 1999. On deep-ocean ^{60}Fe as a fossil of a near-earth supernova. New Astronomy 4, 419–430.
Fields, B.D., Ellis, J.R., Binns, W.R., Breitschwerdt, B., de Nolfo, G.A., Diehl, R., Dwarkadas, V.V., Ertel, A., Faestermann, T., Feige, J., Fitoussi, C., Frisch, P., Graham, D., Haley, B., Heger, A., Hillebrandt, W., Israel, M.H., Janka, T., Kachelriess, M., Korschinek, G., Limongi, M., Lugaro, M., Marinho, F., Melott, A., Mewaldt, R.A., Miller, J., Ogliore, R.C., Paul, M., Paulucci, L., Pecaut, M., Rauch, B.F., Rehm, K.E., Schulreich, M., Seitenzahl, I., Sorensen, M., Thielemann, F.-K., Timmes, F.X., Thomas, B.C., Wallner, A., 2019. Near-Earth Supernova Explosions: Evidence, Implications, and Opportunities. The 2020 Decadal Survey on Astronomy and Astrophysics. arXiv:1903.04589v.
Fields, B.D., Hochmuth, K.A., Ellis, J., 2005. Deep-ocean crusts as telescopes: using live radioisotopes to probe supernova nucleosynthesis. Astrophys. J. 621, 902–907.
Fimiani, L., Cook, D.L., Faestermann, T., Gómez-Guzmán, J.-M., Hain, K., Herzog, G., Knie, K., Korschinek, G., Ludwig, P., Park, J., Reedy, R.C., Rugel, G., 2016. Interstellar ^{60}Fe on the surface of the moon. Phys. Rev. Lett. 116, 1–4.
Fitoussi, C., Raisbeck, G.M., Knie, K., Korschinek, G., Faestermann, T., Goriely, S., Lunney, D., Poutivtsev, M., Rugel, G., Waelbroeck, C., Wallner, A., 2008. Search for supernova-produced ^{60}Fe in a marine sediment. Phys. Rev. Lett. 101, 1–4.
Fry, B.J., Fields, B.D., Ellis, J., 2015. Astrophysical shrapnel: discriminating among near-Earth stellar explosion sources of live radioactive isotopes. Astrophys. J. 800. 17 pp.
Graham, D.W., Hanan, B.B., Hémond, C., Blichert-Toft, J., Albarède, F., 2014. Helium isotopic textures in Earth's upper mantle. Geochem. Geophys. Geosyst. 15, 2048–2074.
Higgins, S.M., Andersen, R.F., Marcantonio, F., Schlosser, P., Stute, M., 2002. Sediment focusing creates 100-ka cycles in interplanetary dust accumulation on the Ontong Java Plateau. Earth Planet. Sci. Lett. 203, 383–397.
Hofmann, A.W., 1988. Chemical differentiation of the Earth: the relationship between mantle, continental crust and oceanic crust. Earth Planet. Sci. Lett. 90, 297–314.
Knie, K., Korschinek, G., Faestermann, T., Wallner, C., Scholten, J., Hillenbrandt, W., 1999. Indication for supernova-produced ^{60}Fe activity on Earth. Phys. Rev. Lett. 83, 18–21.

Knie, K., Korschinek, G., Faestermann, T., Rugel, G., Wallner, A., 2004. ^{60}Fe anomaly in a deep-sea manganese crust and implications for a nearby supernova source. Phys. Rev. Lett. 93, 1–4.
Koll, D., Korschinek, G., Faestermann, T., Gómez-Guzmán, J.M., Kipfstuhl, S., Merchel, S., Welch, J.M., 2019. Interstellar ^{60}Fe in Antarctica. Phys. Rev. Lett. 123, 072701.
Kolla, V., Biscaye, P.E., 1977. Distribution and origin of quartz in the sediments of the Indian Ocean. J. Sediment. Petrol. 47, 642–649.
Limongi, M., Chieffi, A., 2003. Evolution, explosion, and nucleosynthesis of core-collapse supernovae. Astrophys. J. 592, 404–433.
Limongi, M., Chieffi, A., 2006. The nucleosyntheis of ^{26}Al and ^{60}Fe in solar metallicity stars extending in mass from 11 to 120 M the hydrostatic and explosive contributions. Astrophys. J. 647, 483–500.
Love, S.G., Brownlee, D.E., 1993. A direct measurement of the terrestrial mass accretion rate of cosmic dust. Science 262, 550–553.
Ludwig, P., Bishop, S., Egli, R., Chernenko, V., Deneva, B., Faestermann, T., Famulok, N., Fimiani, L., Gómez-Guzmána, J., Haina, K., Korschinek, G., Hanzlik, M., Merchel, S., Rugel, G., 2016. Time-resolved 2-million-year-old supernova activity discovered in Earth's microfossil record. Proc. Natl. Acad. Sci. 113, 9232–9237.
Marcantonio, F., Kumar, N., Stute, M., Anderson, R.F., Seidl, M.A., Schlosser, P., Mix, A., 1995. A comparative study of accumulation rates derived by He and Th isotope analysis of marine sediments. Earth Planet. Sci. Lett. 133, 549–555.
Marcantonio, F., Andersen, R.F., Stute, M., Kumar, N., Schlosser, P., Mix, A., 1996. Extraterrestrial ^{3}He as a tracer of marine sediment transport and accumulation. Nature 383, 705–707.
Marcantonio, F., Higgins, S., Anderson, R.F., Stute, M., Schlosser, P., Rasbury, E.T., 1998. Terrigenous helium in deep-sea sediments. Geochim. Cosmochim. Acta 62, 1535–1543.
Marcantonio, F., Turekian, K.K., Higgins, S., Anderson, R.F., Stute, M., Schlosser, P., 1999. The accretion rate of extraterrestrial ^{3}He based on ^{230}Th flux and the relation to Os isotope variation over the past 200,000 years in an Indian Ocean core. Earth Planet. Sci. Lett. 170, 157–168.
Marcantonio, F., Anderson, R.F., Higgins, S., Stute, M., Schlosser, P., Kubik, P., 2001. Sediment focusing in the central equatorial Pacific Ocean. Paleoceanography 16, 260–267.
McGee, D., Mukhopadhyay, S., 2013. Extraterrestrial He in sediments: from recorder of asteroid collisions to timekeeper of global environmental changes. In: Burnard, P.G. (Ed.), The Noble Gases as Geochemical Tracers. Springer, Berlin, pp. 155–176.
McGee, D., Marcantonio, F., McManus, J.F., Winckler, G., 2010. The response of excess ^{230}Th and extraterrestrial ^{3}He to sediment redistribution at the Blake Ridge, western North Atlantic. Earth Planet. Sci. Lett. 299, 138–149.
McGee, D., Winckler, G., Borunda, A., Serno, S., Anderson, R.F., Recasens, C., Bory, A., Gaiero, D., Jaccard, S.L., Kaplan, M., McManus, J.F., 2016. Tracking eolian dust with helium and thorium: impacts of grain size and provenance. Geochim. Cosmochim. Acta 175, 47–67.
Melott, A.L., Thomas, B.C., Kachelrieß, M., Semikoz, D.V., Overholt, A.C., 2017. A supernova at 50 pc: effects on the Earth's atmosphere and biota. Astrophys. J. 840, 1–9.
Middleton, J.L., Mukhopadhyay, S., Langmuir, C.H., McManus, J.F., Huybers, P.J., 2018. Millennial-scale variations in dustiness recorded in Mid-Atlantic sediments from 0 to 70 ka. Earth Planet. Sci. Lett. 482, 12–22.
Middleton, J.L., Mukhopadhyay, S., Costa, K.M., Pavia, F.J., Winckler, G., McManus, J. F., D'Almeida, M., Langmuir, C.H., Huybers, P.J., 2020. The spatial footprint of hydrothermal scavenging on 230Th_{XS}-derived mass accumulation rates. Geochim. Cosmochim. Acta 272, 218–234.
Morth, C.-M., Backman, J., 2011. Practical steps for improved estimates of calcium carbonate concentrations in deep sea sediments using coulometry. Limnol. Oceanogr.: Methods 9, 565–570.
Mukhopadhyay, S., Farley, K.A., 2006. New insights into the carrier phase(s) of extraterrestrial ^{3}He in geologically old sediments. Geochim. Cosmochim. Acta 70, 5061–5073.
Nier, A.O., Schlutter, D.J., 1990. Helium and neon istopes in stratospheric particles. Meteorit 25, 263–267.
Nier, A.O., Schlutter, D.J., 1993. The thermal history of interplanetary dust particles collected in the Earth's stratosphere. Meteorit 28, 675–680.
Patterson, D.B., Farley, K.A., 1998. Extraterrestrial ^{3}He in seafloor sediments: evidence for correlated 100 kyr periodicity in the accretion rate of interplanetary dust, orbital parameters and Quaternary climate. Geochim. Cosmochim. Acta 62, 3669–3682.
Patterson, D.B., Farley, K.A., Schmitz, B., 1998. Preservation of extraterrestrial ^{3}He in 480-Ma-old marine limestones. Earth Planet. Sci. Lett. 163, 315–325.
Patterson, D.B., Farley, K.A., Norman, M.D., 1999. ^{4}He as a tracer of continental dust: A 1.9 million year record of aeolian flux to the west equatorial Pacific Ocean. Geochim. Cosmochim. Acta 63, 615–625.
Pepin, R.O., Palma, R.L., Schlutter, D.J., 2000. Noble gases in interplanetary dust particles I: the excess helium-3 problem and estimates of the relative fluxes of solar wind and solar energetic particles in interplanetary space. Meteor. Planet. Sci. 35, 495–504.
Pepin, R.O., Palma, R.L., Schlutter, D.J., 2001. Noble gases in interplanetary dust particles II: excess helium-3 in cluster particles and modeling constraints on interplanetary dust particle exposures to cosmic-ray irradiaton. Meteor. Planet. Sci. 36, 1515–1534.
Peucker-Ehrenbrink, B., Ravizza, G., 2000. The effects of sampling artifacts on cosmic dust flux estimates: a reevaluation of nonvolatile tracers (Os, Ir). Geochim. Cosmochim. Acta 64, 1965–1970.
Peucker-Ehrenbrink, B., Ravizza, G., Winckler, G., 2016. Geochemical tracers of extraterrestrial matter in sediments. Elements 12, 191–196.
Piketh, S.J., Tyson, P.D., Steffen, W., 2000. Aeolian transport from southern Africa and iron fertilization of marine biota in the South Indian Ocean. S. Afr. J. Sci. 96, 244–246.
Raiswell, R., Canfield, D.E., 2012. The iron biogeochemical cycle past and present. Geochem. Perspect. 1, 1–220.
Rauscher, T., Heger, A., Hoffman, R.D., Woosley, S.E., 2002. Nucleosynthesis in massive stars with improved nuclear and stellar physics. Astrophys. J. 576, 323–348.
Reedy, R.C., 1987. Nuclide production by primary cosmic-ray protons. J. Geophys. Res. 92, E697–E702.
Rugel, G., Faestermann, T., Knie, K., Korschinek, G., Poutivtsev, M., Schumann, D., Kivel, N., Gunther-Leopold, I., Weinrich, R., Wohlmether, M., 2009. New measurement of the ^{60}Fe half-life. Phys. Rev. Lett. 103, 1–4.
Serno, S., Winckler, G., Anderson, R.F., Hayes, C.T., McGee, D., Machalett, B., Ren, H., Straub, S.M., Gersonde, R., Haug, G.H., 2014. Eolian dust input to the Subarctic North Pacific. Earth Planet. Sci. Lett. 387, 252–263.
Stuart, F.M., Lee, M.R., 2012. Micrometeorites and extraterrestrial He in a ferromanganese crust from the Pacific Ocean. Chem. Geol. 322–323, 209–214.
Svensmark, H., 2012. Evidence of nearby supernovae affecting life on Earth. Mon. Not. R. Astron. Soc. 423, 1234–1253.
Thöle, L.M., Amsler, H.E., Moretti, S., Auderset, A., Gilgannon, J., Lippold, J., Vogel, H., Crosta, X., Mazaud, A., Michel, E., Martínez-García, A., 2019. Glacial-interglacial dust and export production records from the Southern Indian Ocean. Earth Planet. Sci. Lett. 525, 115716.
Thomas, B.C., 2018. Photobiological effects at Earth's surface following a 50 pc supernova. Astrobio 18, 1–10.
Thomas, B.C., Engler, E.E., Kachelrieß, M., Melott, A.L., Overholt, A.C., Semikoz, D.V., 2016. Terrestrial effects of nearby supernovae in the early Pleistocene. Astrophys. J. 826, 1–6.
Torfstein, A., 2012. Size fractionation, reproducibility and provenance of helium isotopes in north-equatorial Pacific pelagic clays. Earth Planet. Sci. Lett. 339–340, 151–163.
Trull, T.W., 1994. Influx and age constraints on the recycled cosmic dust explanation for high ^{3}He/^{4}He ratios at hotspot volcanos. In: Matsuda, J.-.-I. (Ed.), Noble Gas Geochemistry and Cosmochemistry. TerraPub, Tokyo, pp. 77–88.
Wallner, A., Bichler, M., Buczak, K., Dressler, R., Fifield, L.K., Schumann, D., Sterba, J. H., Tims, S.G., Wallner, G., Kutschera, W., 2015. Settling the half-life of ^{60}Fe: fundamental for a versatile astrophysical chronometer. Phys. Rev. Lett. 114, 1–6.
Wallner, A., Feige, J., Koinoshira, N., Paul, M., Fifield, L.K., Golser, R., Honda, M., Linnemann, U., Matsuxaki, H., Merchel, S., Rugel, G., Tims, G., Steier, P., Yamagara, T., Winkler, S.R., 2016. Recent near-Earth supernovae probed by global deposition of interstellar radioactive ^{60}Fe. Nature 532, 69–72.
Wallner, A., Feige, J., Fifield, L.K., Froehlich, M.B., Golser, R., Hotchkis, M.A.C., Koll, D., Leckenby, G., Martschini, M., Merchel, S., Panjkov, S., Pavetich, S., Rugel, G., Tims, S.G., 2020. ^{60}Fe deposition during the late Pleistocene and the Holocene echoes past supernova activity. Proc. Natl. Acad. Sci. 117, 21873–21879.
Winckler, G., Anderson, R.F., Stute, M., Schlosser, P., 2004. Does interplanetary dust control 100 kyr glacial cycles? Quat. Sci. Rev. 23, 1873–1878.
Winckler, G., Anderson, R.F., Fleisher, M.Q., McGee, D., Mahowald, N., 2008. Covariant glacial-interglacial dust fluxes in the equatorial Pacific and Antarctica. Science 320, 93–96.
Winckler, G., Fischer, H., 2006. 30,000 years of cosmic dust in Antarctic ice. Science 313, 491.
Woosley, S.E., Weaver, T.A., 1995. The evolution and explosion of massive stars. II. Explosive hydrodynamics and nucleosynthesis. Astrophys. J. Suppl. 101, 181–235.
Zucker, C., Goodman, A.A., Alves, J., Bialy, S., Foley, M., Speagle, J.S., Groβschedl, J., Finkbeiner, D.P., Burkert, A., Khimey, D., Swiggum, C., 2020. Star formation near the Sun is driven by expansion of the Local Bubble. Nature 601, 334–348.